Structure of the Nucleotide Radical Formed during Reaction of CDP/TTP with the E441Q-22 of E. coli Ribonucleotide Reductase

J|A|C|S ARTICLES

Published on Web 12/18/2008

Structure of the Nucleotide Radical Formed during Reaction of CDP/TTP with the E441Q-α2β2 of *E. coli* Ribonucleotide Reductase

Hendrik Zipse,*,† Erin Artin,‡ Stanislaw Wnuk,§ Gregory J. S. Lohman,‡ Debora Martino,‡ Robert G. Griffin,‡ Sylwia Kacprzak,§ Martin Kaupp,|| Brian Hoffman,⊥ Marina Bennati,§ JoAnne Stubbe,*,‡ and Nicholas Lees*,⊥

Department of Chemistry and Biochemistry, Ludwig-Maximilians Universitaet Muenchen, 81377 Muenchen, Germany, Department of Chemistry, Massachusetts Institute of Technology, Cambridge, Massachusetts 02139, Department of Chemistry, Florida International University, Miami, Florida 33199, Max Planck Institute for Biophysical Chemistry, 37077 Göttingen, Germany, Institute für Physikalische Chemie, Lehrstuhl Albertstraβe 21 D-79104, Freiburg, Germany, and Department of Chemistry, Northwestern University, Evanston, Illinois

Received August 24, 2008; E-mail: stubbe@mit.edu

Abstract: The *Escherichia coli* ribonucleotide reductase (RNR) catalyzes the conversion of nucleoside diphosphates to deoxynucleotides and requires a diferric-tyrosyl radical cofactor for catalysis. RNR is composed of a 1:1 complex of two homodimeric subunits: α and β. Incubation of the E441Q-α mutant RNR with substrate CDP and allosteric effector TTP results in loss of the tyrosyl radical and formation of two new radicals on the 200 ms to min time scale. The first radical was previously established by stopped flow UV/vis spectroscopy and pulsed high field EPR spectroscopy to be a disulfide radical anion. The second radical was proposed to be a 4′-radical of a 3′-keto-2′-deoxycytidine 5′-diphosphate. To identify the structure of the nucleotide radical [1′-^{2}H], [2′-^{2}H], [4′-^{2}H], [5′-^{2}H], [U−^{13}C, ^{15}N], [U−^{15}N], and [5,6 -^{2}H] CDP and [β-^{2}H] cysteine-α were synthesized and incubated with E441Q-α2β2 and TTP. The nucleotide radical was examined by 9 GHz and 140 GHz pulsed EPR spectroscopy and 35 GHz ENDOR spectroscopy. Substitution of ^{2}H at C4′ and C1′ altered the observed hyperfine interactions of the nucleotide radical and established that the observed structure was not that predicted. DFT calculations (B3LYP/IGLO-III/B3LYP/TZVP) were carried out in an effort to recapitulate the spectroscopic observations and lead to a new structure consistent with all of the experimental data. The results indicate, unexpectedly, that the radical is a semidione nucleotide radical of cytidine 5′-diphosphate. The relationship of this radical to the disulfide radical anion is discussed.

Introduction

Ribonucleotide reductases (RNRs) catalyze the conversion of nucleotides to deoxynucleotides in all organisms providing the monomeric precursors required for DNA replication and repair.[1] The *Escherichia coli* class Ia RNR is composed of two subunits: R1 (α_2) and R2 (β_2). Each subunit is homodimeric and a 1:1 complex of α_2 and β_2 is proposed to be the active form of the enzyme. α_2 is structurally homologous to the class II and III RNRs and houses the catalytic machinery required for nucleotide reduction and the binding sites that regulate the specificity and efficiency of substrate turnover. β_2 contains the di-iron-tyrosyl (Y_{122}•) radical cofactor that initiates catalysis on α_2 by a process thought to involve long-range proton coupled electron transfer (PCET).[2,3] The radical propagation process results in generation of a transient thiyl radical (C439•) in the active site of α_2. In addition, there are two cysteines (C225 and C462), a glutamate (E441), and an asparagine (N437) within the active site of α_2 that are essential for catalysis (Scheme 1).

The cysteines provide the reducing equivalents required to make deoxynucleotides,[4,5] the glutamate functions as a general base and general acid catalyst[6] and the asparagine helps to position C225 and E441 in the appropriate conformation to effect the desired chemistry.[7] The mechanism of nucleotide reduction involves transformations employing both nucleotide and protein-derived free radicals.[8] The rate-limiting step in the class Ia RNRs has been shown to be a conformational change that gates the PCET step, masking the chemistry.[9] Studies to

† Ludwig-Maximilians Universitaet Muenchen.
‡ Massachusetts Institute of Technology.
§ Florida International University.
|| Institute für Physikalische Chemie.
⊥ Northwestern University.

(1) Nordlund, P.; Reichard, P. *Annu. Rev. Biochem.* **2006**, *75*, 681–706.
(2) Stubbe, J.; Nocera, D. G.; Yee, C. S.; Chang, M. C. Y. *Chem. Rev.* **2003**, *103*, 2167–2201.
(3) Uhlin, U.; Eklund, H. *Nature* **1994**, *370*, 533–539.
(4) Lin, A. N. I.; Ashley, G. W.; Stubbe, J. *Biochemistry* **1987**, *26*, 6905–6909.
(5) Thelander, L. *J. Biol. Chem.* **1974**, *249*, 4858–4862.
(6) Lenz, R.; Giese, B. *J. Am. Chem. Soc.* **1997**, *119*, 2784–2794.
(7) Karsrayan, A.; Persso, A. L.; Sahlin, M.; Sjoberg, B. M. *J. Biol. Chem.* **2002**, *277*, 5749–5755.
(8) Licht, S.; Stubbe, J. In *Comprehensive Natural Products Chemistry*; Barton, S. D., Nakanishi, K., Meth-Cohn, O., Poulter, C. D., Eds.; Elsevier Science: New York, 1999; Vol. 5, p 163.

10.1021/ja806693s CCC: $40.75

Scheme 1. Working Hypothesis for RNR Catalyzed Reduction of NDPs[a]

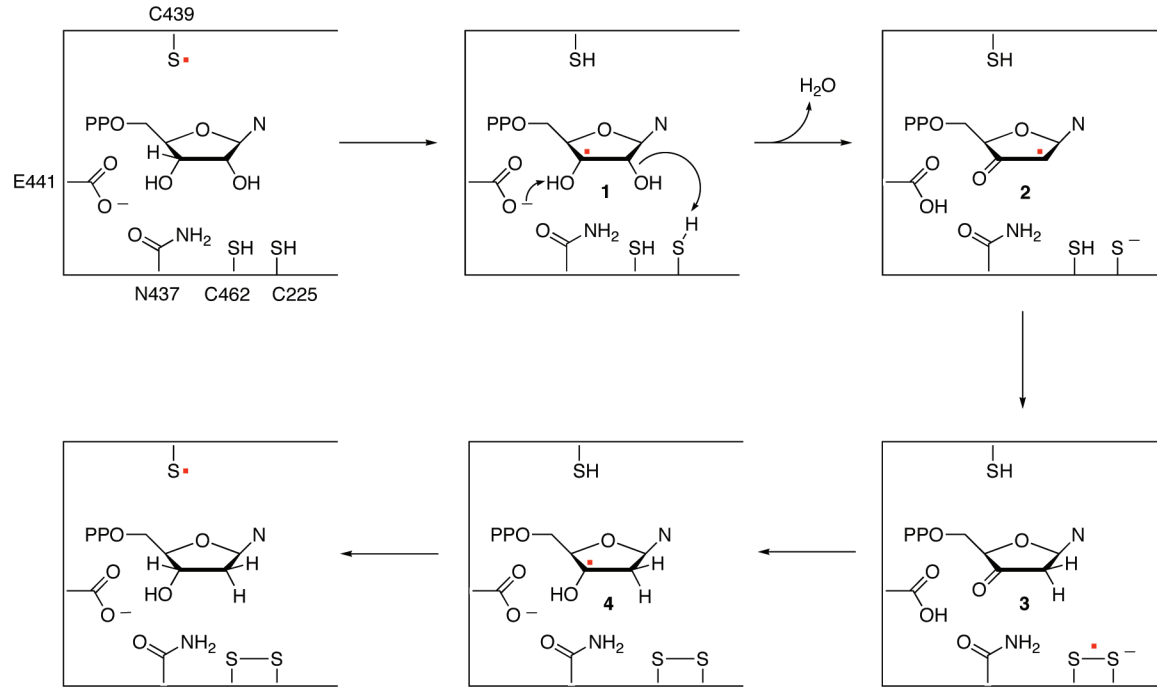

[a] Only α_2 is shown. The C439• is proposed to be generated by the Y122• on β_2. N = A, G, C, or U. C462 and C225 provide the reducing equivalents required to make dNDPs. E441 and N437 have been shown to be essential in catalysis.

examine the chemical mechanism with nucleoside diphosphates (NDPs) and the wild type (wt) RNR met with limited success, because of the rate limiting step.[10] To complement these studies we and others have successfully used mechanism based inhibitors and site-directed protein mutants to perturb the system so that the interesting chemical transformations can be studied.

One Informative Protein Mutant Was E441Q α_2. This mutant is inactive in CDP reduction with either TTP or ATP as allosteric effector. However, kinetic studies of Perrson et al.[11,12] with this mutant, β_2, CDP and TTP, identified two radical species by EPR spectroscopy. Their kinetic analysis led to the model where radical I gave rise to radical II. To assign structures to each radical, a number of isotopic substitution experiments were carried out. Studies using [U-β-^{2}H] cysteine α_2 resulted in altered hyperfine interactions of the first radical monitored by EPR spectroscopy and suggested that this radical was cysteine based. In a second set of experiments [U$-^{13}$C]-CDP replaced CDP. The resulting broadening of the EPR spectrum of the radical II suggested that it was nucleotide based. Their hypothesis based on these studies was that the Y122• in β_2 gave rise to radical I, the C439• in α_2, which then gave rise to the 3′-CDP radical II (Scheme 1, **1**).[12]

Subsequently, the structures of these two radicals were reexamined using high field (140 GHz), pulsed EPR methods.[13] This methodology facilitated deconvolution of the three radicals (Y• and radicals I and II) with superimposed g values and revealed that the cysteine based radical (I) is in fact, a disulfide

Scheme 2. Proposed Outcome when E441Q-α_2 Replaces wt-α_2

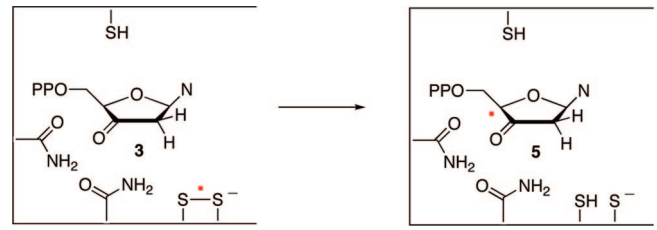

radical and not the C_{439}• initially proposed. Mechanistically this was an important result as our proposed mechanism for nucleotide reduction (Scheme 1), requires that mutation of E441 to a Q, would prevent reduction of intermediate **3** by the disulfide radical anion and hence promote build up of this intermediate.[14,15] Model studies had previously demonstrated that this reduction step requires protonation of the 3′-ketone by E441, concomitant with electron transfer. Identification of a disulfide radical anion thus provided the first insight into the mechanism of reduction of the 3′-ketodeoxynucleotide. In our original report we suggested that radical II was a 4′-ketyl radical of the 3′-deoxynucleotide (**5**, Scheme 2).

The assignment was based on the g values obtained from high field EPR (g_1 = 2.0072, g_2 = 2.0061, and g_3 = 2.0021), and the observation of hyperfine interactions with two nuclei (I = 1/2) originally reported by Perrson et al.[12,13] In the present paper we describe our efforts using isotopically labeled CDP analogs, E441Q α_2, β_2, high field EPR, ENDOR analysis and DFT calculations (B3LYP/IGLO-III/B3LYP/TZVP) to establish the structure of radical II. The structure is not **5** (Scheme 2)

(9) Ge, J.; Yu, G. X.; Ator, M. A.; Stubbe, J. *Biochemistry* **2003**, *42*, 10071–10083.
(10) Stubbe, J.; van der Donk, W. A. *Chem. Rev.* **1998**, *98*, 705–762.
(11) Persson, A. L.; Eriksson, M.; Katterle, B.; Potsch, S.; Sahlin, M.; Sjoberg, B. M. *J. Biol. Chem.* **1997**, *272*, 31533–41.
(12) Persson, A. L.; Sahlin, M.; Sjoberg, B. M. *J. Biol. Chem.* **1998**, *273*, 31016–20.
(13) Lawrence, C. C.; Bennati, M.; Obias, H. V.; Bar, G.; Griffin, R. G.; Stubbe, J. *Proc. Natl. Acad. Sci. U.S.A.* **1999**, *96*, 8979–8984.
(14) Akhlag, M. S.; Murthy, C. P.; Steenken, S.; Von Sonntag, C. *J. Phys. Chem.* **1989**, *93*, 4331–4334.
(15) Schwartz, H. A.; Dodson, R. W. *J. Phys. Chem.* **1989**, *93*, 409–414.

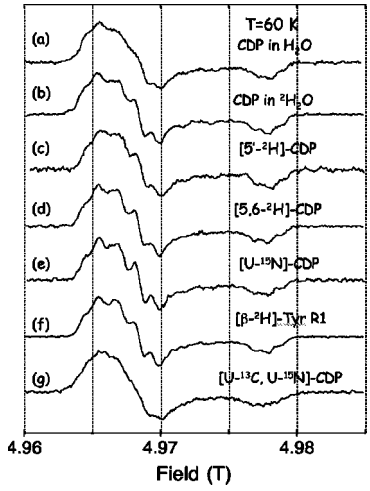

Figure 1. 140 GHz Pulsed EPR spectra of radical II generated from E441Q-α_2/β_2/TTP: (a) with CDP; (b) with CDP and exchange into D_2O; (c) with [5′,5″-^{2}H]-CDP; (d) with [5,6 ^{2}H]-CDP; (e) with [U−^{15}N]-CDP. (f) with [β ^{2}H Y] α_2; and (g) with [U−^{13}C, ^{15}N]-CDP. The spectra were recorded at 70 K. A point by point derivative of the ESE-spectra was built to better visualize the hyperfine structure.

but is proposed to be an off pathway radical with an additional oxygen in the nucleotide (Structure **q**, Figure 6).

Methods and Materials

α_2 and β_2 were isolated as previously described and had specific activities of 2000 μmol/min/mg and 6000 μmol/min/mg respectively.[16] E441Q-α_2 was isolated as previously described. [β-^{2}H] Tyrosine (99% enriched) was obtained from Cambridge Isotopes Laboratory. [U−^{15}N] CDP and [U−^{13}C,^{15}N] CDP were gifts from the Schwalbe laboratory (University of Frankfurt). [2′-^{2}H] cytidine was synthesized by the procedure of Cook and Greenberg[17] NMR analysis revealed 78% deuterium incorporation. [5,6] Dideuterocytidine was synthesized by a modification of the procedure of Rabi and Fox.[18] NMR analysis revealed 83% and 96% incorporation at C-5 and C-6, respectively. For nucleoside chromatography, Merck kieselgel 60-F254 sheets were used for TLC and products were detected by UV or by development of color with $Ce(SO_4)_2$/$(NH_4)6Mo_7O_2$•$4H_2O/H_2SO_4/H_2O$. Merck kieselgel 60 (230−400 mesh) was used for column chromatography. Reagent grade chemicals were used, and solvents were dried and distilled from CaH_2. ^{1}H NMR (400 MHz) was carried out in the Department of Chemistry Instrumentation Facility.

Synthesis of [4′-^{2}H] Cytidine[19] (11b, Scheme 1, SM). 1,2;5,6-Di-*O*-isopropylidene-α-D-allofuranose-4-d (8a).[20,21] 1,2;5,6-Di-*O*-isopropylidene-α-D-*ribo*-hexafuranose-3-ulose (**7a**; 2 g, 7.7 mmol) in D_2O (8 mL) and pyridine (50 mL) was heated for 5 min at 95 °C and then kept at ambient temperature for 20 h. The solvents were removed *in vacuo* and the deuterium exchange procedure repeated five times to achieve deuterium incorporation at >97% (^{1}H NMR). This step was followed by reduction of the oily residue with $NaBH_4$ (0.58 g, 15.38 mmol) in EtOH (20 mL) at 0 °C. After 2 h, excess $NaBH_4$ was decomposed by AcOH (0.5 mL) and the volatiles were evaporated under vacuum. The residue was partitioned between H_2O and CH_2Cl_2 and the water layer was extracted with CH_2Cl_2 (3×). The combined organic layer was washed (brine), dried (Na_2SO_4) and evaporated. The residue was purified by column chromatography (25 → 35% EtOAc/hexanes) to give **8a** (1.44 g, 72%): ^{1}H NMR δ 1.38 (s, 3, CH_3), 1.39 (s, 3, CH_3), 1.48 (s, 3, CH_3), 1.59 (s, 3, CH_3) 4.01−4.12 (m, 3, H5, 6,6′), 4.32 (t, J = 6.5 Hz, 1, H3), 4.64 (dd, J = 3.9, 5.2 Hz, 1, H2), 5.83 (d, J = 3.8 Hz, 1, H1).

3-*O*-Benzoyl-1,2:5,6-di-*O*-isopropylidene-α-D-allofuranose-4-d (8b). Benzoyl chloride (0.67 mL, 0.81 g, 57.5 mmol) was added to a stirred solution of **8a** (1.0 g, 3.83 mmol) in pyridine (8 mL) and stirring was continued for 3 h at ambient temperature. The volatiles were evaporated and the residue was partitioned between EtOAc//$NaHCO_3/H_2O$. The organic layer was separated and was washed (brine), dried (Na_2SO_4), evaporated and purified by column chromatography (8 → 18% EtOAc/hexanes) to give **8b** (1.3 g, 95%): ^{1}H NMR δ 1.35 (s, 3, CH_3), 1.36 (s, 3, CH_3), 1.42 (s, 3, CH_3), 1.57 (s, 3, CH_3), 4.01 (dd, J = 5.8, 8.6. Hz, 1, H6), 4.13 (dd, J = 6.8, 8.6. Hz, 1, H6), 4.38 (t, J = 6.5 Hz, 1, H5), 4.99 (dd, J = 3.9, 5.1 Hz, 1, H2), 5.10 (d, J = 5.1 Hz, 1, H3), 5.91 (d, J = 3.8 Hz, 1, H1), 7.46−7.50 (m, 2, Ar), 7.59−7.63 (m, 1, Ar), 8.07−8.09 (m, 2, Ar).

3-*O*-Benzoyl-1,2-*O*-isopropylidene-α-D-ribofuranose-4-d (9a).[22] H_5IO_6 (225 mg, 0.99 mmol) was added to a stirred solution of **8b** (300 mg, 0.82 mmol) in dried EtOAc (9 mL) at ambient temperature. A precipitate appeared within the first five min and the resulting solution was stirred for 2 h. The precipitate was removed by filtration and was washed with EtOAc (2 × 5 mL). The filtrate was evaporated and the crude 5-aldehyde was dissolved in absolute EtOH (10 mL) and $NaBH_4$ (47 mg, 1.23 mmol) was added. Stirring was continued for 2 h, AcOH (∼0.5 mL) was added and volatiles were evaporated to give **9a** (210 mg, 87%): ^{1}H NMR δ 1.37 (s, 3, CH_3), 1.59 (s, 3, CH_3), 3.74 (d, J = 12.8, Hz, 1, H5), 4.02 (d, J = 12.8 Hz, 1, H5′), 4.97 (t, J = 4.3 Hz, 1, H2), 5.05 (d, J = 4.8 Hz, 1, H3), 5.92 (d, J = 3.7 Hz, 1, H1), 7.29−7.50 (m, 2, Ar), 7.59−7.63 (m, 1, Ar), 8.08−8.10 (m, 2, Ar).

5-*O*-Acetyl-3-*O*-benzoyl-1,2-*O*-isopropylidene-α-D-ribofuranose-4-d (9b). Standard acetylation of **9a** (160 mg, 0.54 mmol) in pyridine (5 mL) with Ac_2O (0.13 mL, 138 mg, 1.36 mmol) gave **9b** (180 mg, 82%; TLC one spot) of sufficient purity to use in next step: ^{1}H NMR δ 1.36 (s, 3, CH_3), 1.58 (s, 3, CH_3), 2.11 (s, 3, CH_3), 4.23 (d, J = 12.3, Hz, 1, H5), 4.45 (d, J = 12.3 Hz, 1, H5′), 4.93 (d, J = 4.6 Hz, 1, H3), 4.97 (t, J = 3.9 Hz, 1, H2), 5.92 (d, J = 3.7 Hz, 1, H1), 7.48−7.50 (m, 2, Ar), 7.60−7.63 (m, 1, Ar), 8.06−8.09 (m, 2, Ar).

1,2,5-Tri-*O*-acetyl-3-*O*-benzoyl-α-D-ribofuranose-4-d (10). A solution of **9b** (180 mg, 0.44 mmol) in CF_3CO_2H/H_2O (9:1, 2.8 mL) was stirred at 0 °C (ice-bath) for 45 min and then the volatiles were evaporated and coevaporated with toluene. The oily residue was dissolved in pyridine (5 mL) and DMAP (3 mg) and Ac_2O (0.21 mL, 224 mg, 2.20 mmol) were added, and the mixture was stirred at ∼5 °C overnight. Volatiles were evaporated and residue was dissolved (EtOAc) and washed (dilute HCl/H_2O, saturated $NaHCO_3/H_2O$, brine), dried (Na_2SO_4) and evaporated. Column chromatography (30% → 35% EtOAc/hexanes) gave **10** (150 mg, 89%; α/β, ∼1:4). The β anomer had: ^{1}H NMR δ 2.10 (s, 3, CH_3), 2.11 (s, 3, CH_3), 2.15 (s, 3, CH_3), 4.25 (d, J = 12.0, Hz, 1, H5), 4.42 (d, J = 12.0 Hz, 1, H5′), 5.50 (dd, J = 1.3, 5.0 Hz, 1, H2) 5.61 (d, J = 4.9 Hz, 1, H3), 6.25 (d, J = 1.3 Hz, 1, H1), 7.47−7.50 (m, 3, Ar), 8.01−8.11 (m, 2, Ar). The α anomer had: ^{1}H NMR δ 2.03 (s, 3, CH_3), 2.12 (s, 3, CH_3), 2.17 (s, 3, CH_3), 4.32 (d, J = 12.1, Hz, 1, H5), 4.39 (d, J = 12.1 Hz, 1, H5′), 5.36 (dd, J = 4.5, 6.4 Hz, 1, H2) 5.55 (d, J = 6.4 Hz, 1, H3), 6.53 (d, J = 4.5 Hz, 1, H1), 7.61−7.65 (m, 3, Ar), 8.09−8.11 (m, 2, Ar).

4-*N*-Acetyl-2′,5′-di-*O*-acetyl-3′-*O*-benzoylcytidine-4′-d (11a). 4-*N*-Acetylcytosine (84 mg, 0.55 mmol) was suspended in hexamethyldisilazane (2 mL) and Me_3SiCl (0.1 mL) was added and the resulting mixture was stirred at 120 °C under argon atmosphere

(16) Salowe, S. P.; Stubbe, J. *J. Bact.* **1986**, *165*, 363–366.
(17) Cook, G. P.; Greenberg, M. *J. Org. Chem.* **1994**, *59*, 4704–4706.
(18) Rabi, J. A.; Fox, J. J. *J. Am. Chem. Soc.* **1973**, *95*, 1628–1632.
(19) Foldesi, A.; Trifonova, A.; Dinya, Z.; Chattopadhyaya, J. *J. Org. Chem.* **2001**, *66*, 6560–6570.
(20) Russel, R. N.; Liu, H. *J. Am. Chem. Soc.* **1991**, *113*, 7777–7778.
(21) Ritchie, R. G. S.; Cyr, N.; Korsch, B.; Koch, H. J.; Perlin, A. S. *Can. J. Chem.* **1975**, *53*, 1424–1433.
(22) Xie, M.; Berges, D. A.; Robins, M. J. *J. Org. Chem.* **1996**, *61*, 5178–5179.

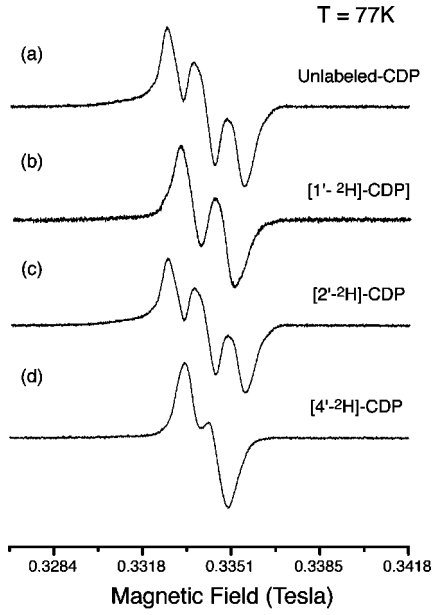

Figure 2. Nine GHz EPR spectra of radical II generated from E441Q-α_2/β_2 /TTP with CDP and [1′-^{2}H], 2′-^{2}H] and [4′-^{2}H]- CDP taken at 77 K and hand quenched at 3 min reaction time. The spectrum of the remaining Y• has been subtracted.

for 4 h. Volatiles were evaporated and the residue was kept under vacuum for 30 min. Compound **10** (140 mg, 0.37 mmol) was dissolved in dry $ClCH_2CH_2Cl$ (4 mL) and this solution and TMSOTf (0.07 mL) were added to the presililated cytosine and the reaction mixture was heated at 70 °C for 7 h under N_2. Volatiles were evaporated and residue was dissolved (EtOAc) and washed ($NaHCO_3$/H_2O, brine), dried (Na_2SO_4) and evaporated. Column chromatography ($CHCl_3$ → 1% MeOH/$CHCl_3$) gave **11a** (130 mg, 75%): ^{1}H NMR δ 2.06 (s, 3, CH_3), 2.17 (s, 3, CH_3), 2.30 (s, 3, CH_3), 4.40 (d, J = 12.5, Hz, 1, H5′), 4.47 (d, J = 12.5 Hz, 1, H5″), 5.57 (t, J = 4.5 Hz, 1, H2′), 5.60 (d, J = 5.8 Hz, 1, H3′), 6.23 (d, J = 4.5 Hz, 1, H1′), 7.44−7.52 (m, 3, H5 and Ar), 7.62 (”t”, J = 7.5 Hz, 1, Ar), 7.95 (d, J = 7.5 Hz, 1, H6) 8.03 (d, J = 7.9 Hz, 2, Ar), 9.55 (brs, 1, NH).

[4′-^{2}H]Cytidine (11b). A solution of **11a** (130 mg, 0.27 mmol) in NH_3/MeOH (10 mL) was stirred at 0 °C for 6 h. Volatiles were evaporated and the residue was dissolved in H_2O and extracted with CH_2Cl_2 (3×) and then with Et_2O. The aqueous layer was concentrated and applied to a column of Dowex 1 × 2−200 (OH^- form). Elution (H_2O → 40% MeOH/H_2O) and concentration of the appropriate fractions gave **11b** (55 mg, 82%) as a white powder (with deuterium incorporation of >98%): ^{1}H NMR (DMSO-d_6) δ 3.52 (dd, J = 5.2, 12.1, Hz, 1, H5′), 3.64 (dd, J = 5.2, 12.1 Hz, 1, H5″), 3.92−3.94 (m, 2, H2′, 3′), 4.96 (d, J = 4.5 Hz, 1, 3′ OH), 5.03 (t, J = 5.1 Hz, 1, 5′ OH), 5.27 (d, J = 4.7 Hz, 1, 2′ OH), 5.70 (d, J = 7.4 Hz, 1, H5), 5.76 (d, J = 3.7 Hz, 1, H1′), 7.12 (br d, J = 6.2 Hz, 2, NH_2), 7.84 (d, J = 7.4 Hz, 1, H6).

[1′-^{2}H cytidine] was prepared as previously described. Deuterium incorporation was 93% based on ^{1}H NMR and ESI-MS.[23]

Synthesis of [5′, 5″-^{2}H]-CDP (20, Figure 2, SM).[19,24] Synthesis of [5′, 5″-^{2}H] CDP was carried out as described in Figure 2 SM. Deuterium incorporation is >98%.

Conversion of Cytidine to CMP and CDP by Human Deoxycytidine Kinase. All isotopically labeled cytidine analogs, except [5′, 5″-^{2}H] cytidine were converted enzymatically to CMP using hexahistidine tagged-human deoxycytidine kinase (hdCK) by a modification of the procedure of Usova and Eriksson.[25] A typical reaction contained in a final volume of 5 mL: 1 mM cytidine, 1.33 mg/mL 6xHis-hdCK (specific activity 170 nmol/mg/min), 2 mM ATP, 2 mM DTT and 0.5 mg/mL BSA in 50 mM Tris, 100 mM KCl, 5 mM $MgCl_2$ at pH 7.6. The reaction was initiated by the addition of enzyme and incubated at 37 °C for 10 min. The reaction mixture was then loaded onto a DEAE Sephadex A25 column (1 × 14 cm) and eluted with a 100 mL × 100 mL linear gradient from 0.005 to 0.4 M triethylammonium bicarbonate (TEAB) pH 7.8. The CMP eluted at 0.2 M TEAB, the appropriate fractions were pooled and the TEAB removed in vacuo. CMP was produced quantitatively.

Phosphorylation of CMP to CDP by Human UMP-CMP Kinase. All isotopically labeled cytidine analogs were converted to CDP using a glutathione S-transferase tagged UMP/CMP kinase by a modification of the procedure of Van Rompay et al.[26] A typical reaction contained in a final volume of 5 mL: 1 mM CMP, 0.065 mg/mL GST-UMP/CMP kinase (specific activity 4.8 μmol/mg/min), 4 mM ATP, 2 mM DTT in 50 mM Tris, 5 mM $MgCl_2$ at pH 8.0. The reaction was initiated by the addition of enzyme and incubated at 37 °C for 30 min. The reaction mixture was then loaded onto a DEAE Sephadex A25 column (1 × 14 cm) and eluted with a 120 mL × 120 mL linear gradient from 0.005 to 0.6 M TEAB. Fractions of 5.3 mL were collected and CMP eluted at 0.4 M TEAB. Those without ADP, were pooled and the TEAB removed in vacuo. CDP is produced in 80% yield.

X Band EPR Spectroscopy of the Reaction of E441Q-α2, β2, and CDP. The reaction mixtures contained in a final volume of 0.23 mL: 45 μM E441Q-α2, 45 μM β2, 1 mM CDP, 0.8 mM TTP, 5 mM DTT, 50 mM HEPES pH 7.6, 15 mM $MgSO_4$, and 1 mM EDTA. All components except for substrate were combined and equilibrated at 25 °C for 5 min. The reaction was started by the addition of CDP and then transferred to an EPR tube and frozen in liquid nitrogen after 1 to 4 min incubation at 25 °C. Continuous wave EPR spectra at 9 GHz were acquired on a Bruker ESP-300 spectrometer equipped with a Bruker high sensitivity 4119HS cylindrical cavity and an ER-041G microwave bridge containing an internal frequency counter. Spectra were acquired at either 77 K using a liquid-helium cooled ESR-900 cryostat and an Oxford LLT 650/1.0 transfer line. Typical parameters were as follows: microwave power 20 μW; modulation frequency 100 kHz; modulation amplitude 1 G; conversion time 20.48 ms; time constant 5.12 ms. The sweep width was 150G and 2048 points were acquired per spectrum.

High Field (140 GHz) EPR Spectroscopy of the Reaction of E441Q-α2, β2, and CDP. The reaction mixture contained in a final volume of 15 μL: 300 μM E441Q-α2, 300 μM β2, 1 mM CDP (or 0.3 mM GDP), 0.8 mM TTP, 5 mM DTT, 50 mM HEPES pH 7.6, 15 mM $MgSO_4$, and 1 mM EDTA. After equilibration of the mixture in the absence of substrate at 25 °C, the reaction was started by the addition of CDP and the mixture was drawn into a suprasil capillary by capillary action and frozen in liquid nitrogen 3 min after initiation. Spectra were acquired at 70 K on a custom-designed pulsed spectrometer.[27] The stimulated echo sequence was used with typical pulse length of $t_{\pi/2}$ = 60 ns and pulse spacing of τ = 200 ns. The pulsed method allowed us to filter out the radical II from the Y•, as previously demonstrated.[13] The external magnetic field was swept with the assistance of a field lock system. The echo intensity at each field position was integrated. The number of shots per point, scans and recycle delays were adjusted for different signal intensities and temperatures.

35 GHz EPR/ENDOR Spectroscopy. Reactions were prepared as described for the 140 GHz experiments except that the final

(23) Lohman, G. J. S., 2006.
(24) Davisson, J. J.; Davis, D. R.; Dixit, V. M.; Poulter, C. D. *J. Org. Chem.* **1987**, *52*, 1794–1801.
(25) Usova, E. V.; Eriksson, S. *Eur. J. Bioch.* **1997**, *248*, 762–766.
(26) Van Rompay, A. R.; Johansson, M.; Karlson, A. *Mol. Pharm.* **1999**, *56*, 562–569.
(27) Bennati, M.; Farrar, C. T.; Bryant, J. A.; Inati, S. J.; Weis, V. J. G. G.; Riggs-Gelasco, P.; Stubbe, J.; Griffin, R. G. *App. Magn. Res.* **1999**, *21*, 389–410.

volume was 60 μL. Pulsed EPR and ENDOR data were obtained at 35 GHz with an instrument[28] described earlier. During the course of experiments several components of the spectrometer were modified. A solid-state 4W microwave amplifier (Microwave Power Inc.) was used in place of the TWTA 40 W amplifier, and data acquisition was handled using the software package SpecMan[29] (http://www.speman.4epr.com) in conjunction with a SpinCore PulseBlaster ESR_PRO 400 MHz word generator and an Agilent Technologies Acquiris DP235 500 MS/sec digitizer. First order ENDOR spectra from $I = 1/2$ nuclei (^{1}H, ^{13}C, ^{15}N) exhibit pairs of features at $\nu_\pm = |\nu_N \pm A/2|$.

Computational Methods. Geometry optimizations and calculation of hyperfine couplings (hfc) have been performed with Gaussian 03 (http://gaussian.com/citation_g03.htm) using the Becke3LYP functional[30] in combination with the TZVP basis set.[31] Thermochemical parameters to predict enthalpies at 298K have been obtained using the unscaled force constants computed at this latter level. Single point calculations have then been performed using the IGLO-III basis sets[32] in combination with the Becke3LYP functional in order to predict isotropic and anisotropic hyperfine coupling (hfc) parameters. These latter calculations use a pruned grid of 99 radial shells and 590 angular points for numerical integration, while all geometry optimizations have been performed with the default pruned 75/302 grid. Spin and charge densities have been calculated using the Natural Population Analysis (NPA)[33] of the B3LYP/IGLO-III//B3LYP/TZVP Kohn−Sham orbitals. Hyperfine tensors for small reference compounds were calculated with the ADF-DFT package to test those obtained from Gaussian 03. The *g*-tensor calculations were carried out on the B3LYP/TZVP optimized structures and employed a second-order perturbation approach,[34] which has been demonstrated to provide excellent accuracy in calculations of *g*-tensors for organic radicals.[35−39] The Kohn−Sham molecular orbitals (MO) were obtained with the TURBOMOLE (v. 5.6) program[40,41] at the RI-BP86/DZVP level. The unrestricted Kohn−Sham molecular-orbital information from TURBOMOLE was transferred by appropriate interface routines to the MAG (magnetic resonance) property module of the in-house program ReSpect.[42] Low symmetry of the structures and a variety of spin distribution patterns together with small *g*-anisotropy imposed use of an explicit description of all one- and two-electron Breit-Pauli spin−orbit integrals (FULL) and distributed gauges with gauge-including atomic orbitals (GIAOs[43,44]). In the calculations, the *g*-tensor is defined as $\boldsymbol{g} = g_e(\mathbf{1}) + \boldsymbol{\Delta g}$, where $g_e = 2.002319$. *g*-Shift components (Δg_i) defined as corrections to the free electron value in ppm (that is, in units of 10^{-6}) are presented and discussed. The approach presented includes not only the dominant second-order spin−orbit/orbital-Zeeman cross terms but also the relativistic mass correction (RMC) and the one-electron part of the spin−orbit gauge correction (GC) terms.[34,39]

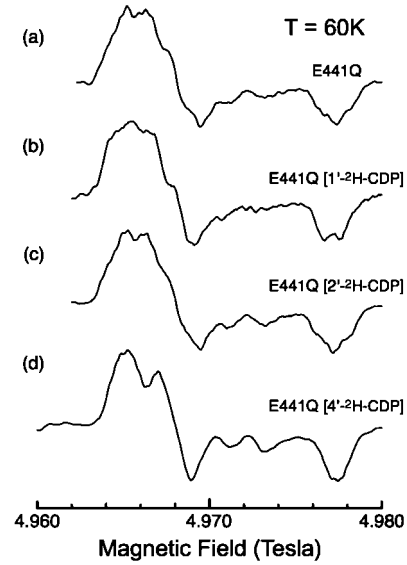

Figure 3. 140 GHz pulsed EPR spectra of radical II generated from E441Q-α_2/β_2/TTP with CDP and [1′-^{2}H], [2′-^{2}H] and [4′-^{2}H]- CDP taken at 60 K and hand quenched 3 min after mixing. The features in the region between 49700 and 49740 (bottom two spectra) are associated with remaining Y• due to difficulty in temperature control during the pulsed experiment.

Results

To test our initial proposal that the 3 min radical is a 4′-ketyl radical[13] and to obtain more experimental information, we generated a series of specifically, isotopically labeled CDPs and investigated the effect of the isotopic substitution on the hyperfine couplings with 9 and 140 GHz EPR spectroscopy. Given our proposed structure for radical II (**5**, Scheme 2) and that the triplet EPR line shape reported by Persson et al. at 9 GHz (see Figure 3) had been attributed to the hyperfine couplings with two almost equivalent protons,[11] we initially examined the effect of selective CDP deuterated at C5′,5″. The synthetic method, reduction of the 5′-aldehyde with NaB^2H_4, resulted in incorporation of a single ^{2}H (>98%), randomly distributed between H5′ and H5″. The results from an experiment with this compound taken at 140 GHz are shown in Figure 1c. No alterations in the observed hyperfine are apparent relative to the control with CDP (Figure 1a). This result demonstrates that radical II is not **5** (Scheme 2) as we had proposed. Such a radical would exhibit substantial hyperfine coupling to at least one of the adjacent protons at C5′ and this coupling would be decreased by deuteration.

Our previous analysis eliminated the possibility that **2** (Scheme 1) was radical II as the observed hyperfine interactions from the protons attached to C1′ and C2′ of **2** must be substantially different, in contrast to the experimental results. To eliminate the possibility that one or both of the hyperfine

(28) Davoust, C. E.; Doan, P. E.; Hoffman, B. M. *J. Magn. Reson.* **1996**, *119*, 38–44.
(29) Epel, B.; Gromov, I.; Stoll, S.; Schweiger, A.; Goldfarb, D. *Concepts Magn. Reson., Part B* **2005**, *26B*, 36–45.
(30) Becke, A. D. *J. Chem. Phys.* **1993**, *98*, 5648–5652.
(31) Schaefer, A.; Huber, C.; Ahlrichs, R. *J. Chem. Phys.* **1994**, *100*, 5829–5835.
(32) Kutzelnigg, W.; Fleischer, U.; Schindler, M. In *NMR: Basis Principles and Progress*; Diehl, P., Fluck, E., Günther, H., Kosfeld, R., Seelig, J., Eds.; Springer: Berlin, 1990.
(33) Himo, F.; Siegbahn, P. E. M. *J. Phys. Chem. B* **2000**, *104*, 7502–7509.
(34) Malkina, O. L.; Vaara, J.; Schimmelpfennig, B.; Munzarova, M.; Malkin, V. G.; Kaupp, M. *J. Am. Chem. Soc.* **2000**, *122*, 9206–9218.
(35) Ciofini, I.; Reviakine, R.; Arbuznikov, A.; Kaupp, M. *Theo. Chem. Acc.* **2004**, *111*, 132–140.
(36) Kacprzak, S.; Kaupp, M.; MacMillan, F. *J. Am. Chem. Soc.* **2006**, *128*, 5659–5671.
(37) Kaupp, M.; Gress, T.; Reviakine, R.; Malkina, O. L.; Malkin, V. G. *J. Phys. Chem. B* **2003**, *107*, 331–337.
(38) Kaupp, M.; Remenyi, C.; Vaara, J.; Malkina, O. L.; Malkin, V. G. *J. Am. Chem. Soc.* **2002**, *124*, 2709–2722.
(39) Kaupp, M.; Reviakine, R.; Malkina, O. L.; Arbuznikov, A.; Schimmelpfennig, B.; Malkin, V. G. *J. Comput. Chem.* **2002**, *23*, 794–803.
(40) Ahlrichs, R.; Bar, M.; Haser, M.; Horn, H.; Kolmel, C. *Chem. Phys. Lett.* **1989**, *162*, 165–169.
(41) Ahlrichs, R.; von Arnim, M. In *Methods and Techniques in Computational Chemistry*; Clementi, E., Corongiu, G., Eds. 1995; p 509.
(42) Malkin, V. G.; Malkina, O. L.; Reviakine, R.; Arbuznikov, A. V.; Kaupp, M.; Schimmelpfennig, B.; Malkin, I.; Helgaker, T.; Ruud, K. 2003.
(43) Ditchfie, R. *Mol. Phys.* **1974**, *27*, 789–807.
(44) Wolinski, K.; Hinton, J. F.; Pulay, P. *J. Am. Chem. Soc.* **1990**, *112*, 8251–8260.

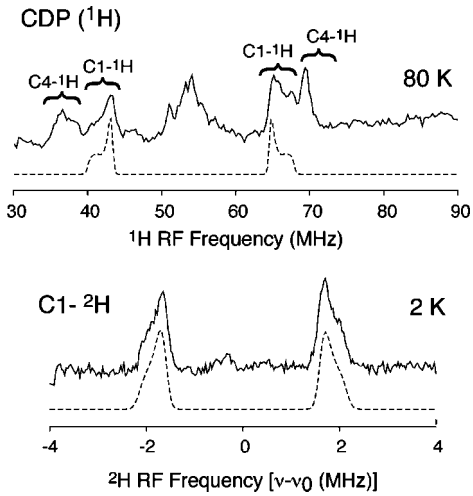

Figure 4. 35 GHz Pulsed Davies ^{1}H (top) and ^{2}H (bottom) ENDOR spectra of radical II generated from E441Q-α_2/β_2/TTP with CDP and [1′-^{2}H]-CDP hand quenched 3 min after mixing. Simulation of C1′-^{1},^{2}H peaks. Experimental conditions: Davies ENDOR π pulse lengths 80 ns, τ = 800 ns, RF pulse length 20 μs, repetition rate 5 ms, 15,000 transients/point. reMims ENDOR π /2 pulse lengths 32 ns, τ = 144 ns, RF pulse length 60 ms, repetition rate 20 μs, 192 transients/point. Simulation parameters: ^{1}H(top) A = [21.5, 21.5, 28] MHz, α = 45°, line width = 0.5 MHz. ^{2}H(bottom) A = [3.3, 3.3, 4.3] MHz, α = 45°; P = 0.08 MHz and line width = 0.2 MHz.

interactions is associated with an exchangeable proton, an experiment in D_2O with CDP was carried out.[8] No changes in the hyperfine structure were observed (Figure 1b), except for the expected sharpening due to the exchange of the protein matrix protons, eliminating this possibility.

The unusual g values of radical II and our previous identification of a 3′-ketone during catalysis,[45] seemed to leave few options for assignment of nuclei giving rise to the observed hyperfine interactions. One option was that the nucleic acid base could interact with the sugar radical resulting in the delocalization of the radical onto the base.[46] This proposal seemed unlikely as Perrson had reported (no data was shown) that interaction of E441Q-α_2 with GDP/TTP gave rise to a similar radical and a purine base is distinctly different from the pyrimidine base. However, at this stage, the identity of II was a real mystery, thus the importance of the base was further investigated using [5, 6-^{2}H], [U−^{15}N], [U−^{13}C, ^{15}N] CDP with E441Q-α_2. Once again as revealed in Figure 1d and e no altered hyperfine interactions were observed. The spectrum with [U−^{13}C, ^{15}N]-CDP (Figure 1g) was slightly broadened reproducing the previous results described by Perrson and requiring that II is nucleotide based.[11]

Finally, previous studies on galactose oxidase, an enzyme with a *o*-thioether substituted tyrosyl radical essential for catalysis, revealed a spectrum very similar to that of radical II.[47] One could image a scenario where a similar radical could be generated given the importance of the C439 radical in nucleotide reduction and its propinquity to Y730 (Scheme 1). Thus, based on previous studies with galactose oxidase, we incorporated [β-^{2}H] tyrosine into all of the tyrosines of E441Q-α_2. The results of incubation of this protein with CDP, Figure 1f, revealed no altered hyperfine structure.

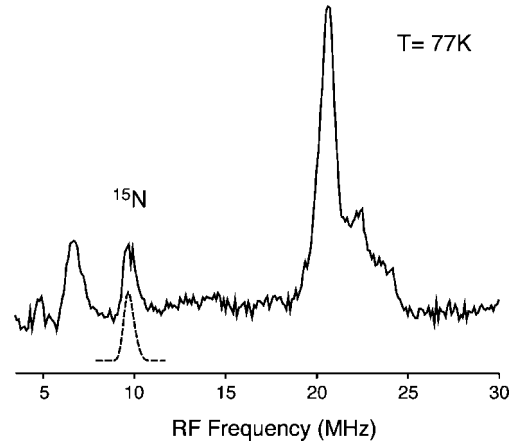

Figure 5. 35 GHz ENDOR spectrum at 77 K of E441Q-α_2/β_2/TTP and [U−^{13}C/^{15}N] CDP; (---) simulation of the ^{15}N peak. Experimental conditions: π pulse lengths 80 ns, τ = 800 ns, RF pulse length 20 μs, repetition rate 5 ms, 10000 transients/point. Simulation parameters: A = [8.0, 8.0, 9.5] MHz, line width = 0.5 MHz.

At this point we believed we had a nucleotide based radical, but that it was probably generated off pathway or in a parallel pathway relative to the disulfide radical anion formation and not directly from the disulfide radical anion as Perrson et al. proposed.[12] We thus synthesized 1′, 2′, 4′-[^{2}H] CDPs and examined the spectra resulting from these compounds at both 9 and 140 GHz by EPR spectroscopy. The results are shown in Figures 2 and 3.

Deuteration at either C1′ or C4′ collapses the triplet to a doublet (compare Figure 2a with b and d and Figure 3a with b and d), while no such collapse occurs by deuteration at C2′ (compare Figure 2a and c and Figure 3a and c). These surprising findings suggest that the radical structure is unusual and led us to search for other possible couplings to protons, carbons, and nitrogens in more detail in the effort to determine the structure.

ENDOR ^{1}H. The EPR measurements assigned the two protons giving rise to the triplet EPR pattern as those associated with C1′, C4′ of CDP. To obtain precise measurements of their hyperfine coupling tensors, 35 GHz ^{1}H Davies and ^{2}H Mims and reMims[48,49] ENDOR studies were carried out on II prepared with unlabeled CDP and with C1′-^{2}H labeled CDP (Figure 4). The ^{1}H spectra collected at 2 K (not shown) are dominated by ^{1}H peaks from Y•, which overlap all the signals associated with radical II except that from C4′-^{1}H. However, at 80 K the phase memory of Y• is shorter than that of II and Y• does not contribute to the Davies ^{1}H pulsed ENDOR spectra collected with a pulse spacing τ = 800 ns. The 80 K ^{1}H spectrum of unlabeled II shows intensity from ν_+ of the two strongly coupled protons with 64 $\lesssim \nu_+ \lesssim$ 71 MHz, and with corresponding ν_- intensity (Figure 4, top). ^{2}H spectra collected at 2K from the radical with [1′−^{2}H] CDP (Figure 4, bottom) isolate the ^{2}H signal from that site. Simulations of the ^{2}H pattern yielded the hyperfine tensor, $\mathbf{A}$(C1′−^{1}H) = [21.5, 21.5, 28] MHz.

The remaining ^{1}H ENDOR intensity from the strongly coupled protons must come from C4′-^{1}H; it has larger couplings, with maximum and minimum hyperfine tensor values of A = 38, 30 MHz. A more detailed analysis was not feasible. The observation of large and roughly isotropic hyperfine couplings

(45) Ator, M. A.; Stubbe, J. *Biochemistry* **1985**, *24*, 7214–21.
(46) Schiemann, O.; Feresin, E.; Carl, T.; Giese, B. *ChemPhysChem* **2004**, *5*, 270–274.
(47) Gerfen, G. J.; Bellew, B. F.; Griffin, R. G.; Singel, D. J.; Ekberg, C. A.; Whittaker, J. W. *J. Phys. Chem.* **1996**, *100*, 16739–16748.
(48) Doan, P. E.; Hoffman, B. M. *Chem. Phys. Lett.* **1997**, *269*, 208–214.
(49) Schweiger, A.; Jeschke, G. *Principles of Pulse Electron Paramagnetic Resonance*; Oxford University Press: Oxford, UK, 2001.

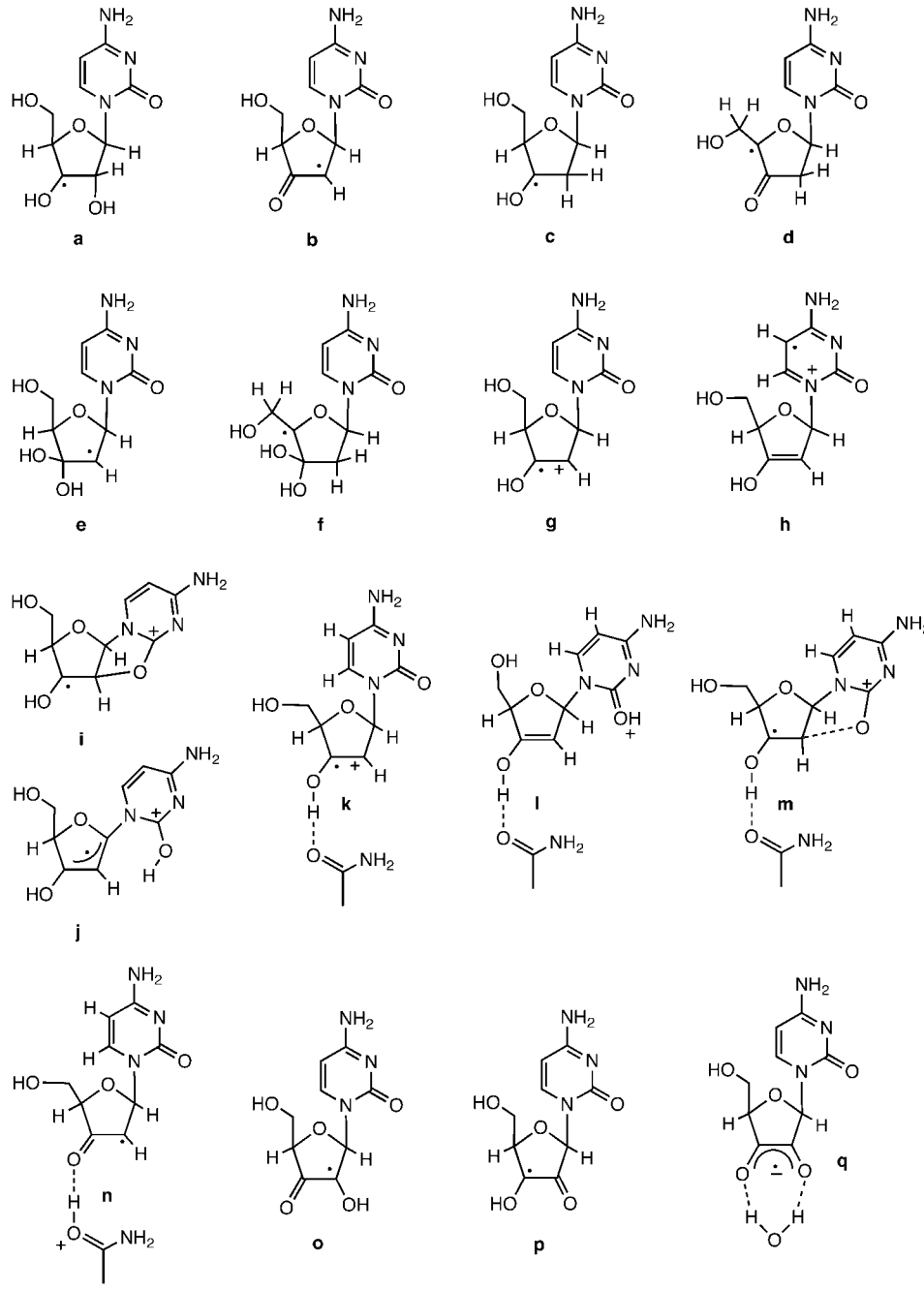

Figure 6. Structures considered for II in the quantum chemical calculations.

to C1′−^{1}H and C4′−^{1}H suggest that these protons are adjacent to sites of substantial spin density.

To search for possible smaller couplings to the C2′ or C5′ protons, ^{2}H Mims spectra were collected on samples prepared with [C2′−^{2}H] CDP and [C5′−^{2}H] CDP (not shown). The search was hampered by the presence of ($\Delta M_I = 2$) nitrogen peaks in the region of the deuteron larmor frequency, but nonetheless, no ^{2}H peaks were seen for [C2′−^{2}H]. Only very weak possible peaks were seen for [C5′−^{2}H] at a $\tau = 800$ ns; if real, these would correspond to a ^{2}H coupling of ∼0.2 MHz (corresponding to a ^{1}H coupling of ∼1.3 MHz). Overall, the ^{2}H experiments definitively establish that no protons, other than those associated with C1′−^{1}H or C4′−^{1}H, have a coupling larger than ∼2 MHz.

^{15}N/^{13}C: The 35 GHz Davies pulsed ENDOR spectrum of a sample with [U−^{13}C, U−^{15}N] CDP at ∼80 K is shown in Figure 5. Peaks are observed at ∼5 (weak), 6−7, 10, 20, and 22 MHz, and an "edge" at ∼ 24 MHz. None of these features are seen in an unlabeled sample, demonstrating that they are all due to coupling to ^{13}C/^{15}N of the substrate. The assignment of these features is tricky. First, the 10 and 20 MHz peaks are separated exactly $2\nu(^{15}\mathrm{N})$; suggesting an assignment to a ^{15}N doublet centered at $A(^{15}\mathrm{N})/2 \approx 15$ MHz. However, such a doublet would correspond to a ^{14}N coupling in the unlabeled sample of $A(^{14}\mathrm{N}) \approx 21$ MHz. Such an ^{14}N would have given rise to observable features in ENDOR spectra of the unlabeled CDP and would have prevented observation of the well-resolved triplet in the EPR spectrum of the unlabeled radical, Figure 2a. Thus, we reject the assignment of the 20 MHz peak to ^{15}N. Similar arguments lead us to reject the assignment of features between 20 and 24 MHz to ^{15}N. Thus, we assign the ENDOR intensity between 20 and 24 MHz to ν_+ features from ^{13}C with $14 < A$

Table 1. Calculated g-Tensors and Isotropic Fermi-Contact Couplings (in Gauss) for Selected Hydrogen Atoms for All Systems Shown in Figure 6[a]

	g-tensor components				isotropic hfc (Gauss)				
structure	g_{11}	g_{22}	g_{33}	g_{av}	H(C1′)	H(C2′)	H(C4′)	H(C5′)	other
a	2.0022	2.0032	2.0042	2.0032	−0.8	+28.5	+20.6	+0.4 +0.6	
b	2.0023	2.0038	2.0097	2.0052	+24.0	−16.7	−0.2	+0.4 −0.01	
c	2.0021	2.0032	2.0039	2.0030	−0.6	+33.8 +13.0	+22.7	−0.4 −0.7	
d	2.0021	2.0054	2.0071	2.0049	+2.8	+3.9 +1.9	−	+12.6 +0.1	
e	2.0021	2.0025	2.0026	2.0024	+30.7	−20.0	+1.2	−0.1−0.1	
f	2.0026	2.0031	2.0040	2.0031	+6.8	+1.6 +0.7	−	+0.3 +9.5	
g	2.0022	2.0039	2.0047	2.0036	+8.3	−1.8	+14.1	−0.5 +0.9	
h	2.0028	2.0043	2.0076	2.0049	+1.0	−1.8	+1.3	+0.1 −0.1	−11.6 (H(C5)) +1.6 (H(C6))
i	2.0022	2.0030	2.0039	2.0030	+1.0	+17.3	+21.0	+0.6 −1.0	
j	2.0021	2.0036	2.0038	2.0032	−	+2.3	+21.9	−0.2 −0.7	+0.2 (H(OC2))
k	2.0032	2.0046	2.0065	2.0047	+1.0	−7.2	+5.0	−0.3 −0.1	−5.7 (H(C5))
l	2.0038	2.0059	2.0070	2.0056	+80.4	−6.3	+21.8	+2.4 −0.7	
m	2.0026	2.0043	2.0047	2.0039	+7.5	−0.7	+9.7	−0.1 −0.5	
n	2.0022	2.0043	2.0058	2.0041	+21.0	−12.8	+3.4	−0.13 +0.04	
o	2.0022	2.0046	2.0072	2.0047	+20.6	−	+3.3	−0.3 −0.1	
p	2.0021	2.0045	2.0074	2.0047	+4.5	−	+21.7	−0.5 −0.7	
q	2.0022	2.0062	2.0076	2.0053	+8.3	−	+8.0	−0.3 −0.3	
exp.	2.0021	2.0061	2.0072	2.0051	two couplings (8.5, 11.4 Gauss) to C1′/C4′				

[a] The protons for which the hfc are computed are marked in Figure 6.

< 22 MHz. Attempts to simulate this signal in terms of a single ^{13}C failed, so we conclude that it arises from at least two strongly coupled ^{13}C. Given these conclusions, it is plausible to assign the 7 and 5 MHz peaks as their ν- partners.[50] Additional Mims ENDOR measurements do not support an alternate assignment of these peaks as a ν_+/ν_- doublet from a weakly coupled ^{15}N. With these assignments, then the 10 MHz peak can only be a $\nu+$ peak from ^{15}N with A ∼9 MHz; its ν_- partner is at ∼1 MHz, and not detected. As shown in Figure 5, this peak can be simulated as arising from a nearly isotropic ^{15}N coupling, ^{15}N hyperfine tensor A = [8.0, 8.0, 9.5] MHz.[51] In addition Mims ENDOR spectra (Supporting Information, Figure 5) show weak signals near the ^{13}C and ^{15}N Larmor frequencies that correspond to ^{3}C and ^{15}N with very small coupling(s), A ≤ 0.5 MHz.

To summarize, the ^{1}H ENDOR and EPR measurements suggest that C1′ and C4′ are adjacent to sites with substantial spin density, while the ^{13}C/^{15}N measurements show that the spin density of II is distributed so as to give relatively strong hyperfine couplings to at least two ^{13}C and one ^{15}N nucleus. However, with multiple labels in a single CDP, the measurements do not define the sites involved. Further, the spin density required to generate the observed signals would be a small fraction of an electron; to locate this spin density and to constrain a structure assignment, more nuclear couplings are required. *In principle*, the problem could be solved by the synthesis of CDP with additional, specific labels (^{13}C, ^{15}N, ^{17}O, ^{2}H), but this is chemically impractical. As a result, quantum chemical calculations were undertaken.

Quantum Chemical Calculations Propose a Structure for II. A new model structure is required to explain the equivalency of the ^{1}H hyperfine couplings associated with C1′ and C4′ and the observed g values. Initially we focused on model systems descriptive of plausible intermediates in the reaction of CDP with E441Q-RNR (Figure 6, **a**−**m**). The hyperfine couplings (hfc) and g-tensor data were calculated. These models differ from the actual substrates as the phosphate groups have been removed from C5′. To avoid artifacts caused by the truncation, conformational searches excluded all structures in which the C5′ hydroxyl group acted as a hydrogen bond donor. The energetically most favorable conformers have been used for the calculation of spectroscopic data. The first three models **a**−**c** correspond to transient intermediates proposed for the normal mechanism of nucleotide reduction. Their calculated hfc data (Table 1) differ substantially from those measured for II. The C3′-keto radical **d** (Figure 6) was included here as a model for the off-pathway radical **5** (Scheme 2) and was previously examined computationally by Siegbahn et al.[33] While their results clearly favored formation of radical **d** on thermodynamic grounds, their analysis failed to recapitulate the observed experimental g-factor and hfc pattern. Our calculations also suggested that the hydrated versions of the two keto-substituted radicals **b** and **d**, **e** and **f**, are not good candidates for II.

As shown in Scheme 1, a primary function of the E441 carboxylate involves deprotonation of the C3′ hydroxyl group. Should this deprotonation step be impaired in the E441Q mutant one might expect formation of radical cation **g** (instead of radical **b**) in the course of the reaction. This species shows hyperfine couplings to the hydrogens at C1′ and C4′ similar to those measured experimentally, but lacks the proper g-factor characteristics. The lifetime of radical cations such as **g** may also be limited, as conformational searches induced a number of side reactions with minimal to no enthalpic barrier. The products formed on this occasion include the base radical cation **h**, the cyclized radical cation **i**, and the allylic, distonic radical cation **j**. Isomer **j** is the energetically most favorable of these radical cations, the isomers **g**, **i** and **h** being less stable by 15.2, 16.9, and 65.4 kJ/mol, respectively, at the UB3LYP/TZVP level of theory. The calculated spectroscopic data of **j** are, however, far from experimental values.

The most relevant interaction between a radical cation such as **g** with the mutant enzyme binding pocket will most likely involve the Q441 amide side chain and calculations on radical cations **g**−**j** have therefore been repeated using acetamide as a mimic for this side chain. The energetically most favorable structure obtained in this system was **n**, in which proton transfer has occurred from the radical cation to acetamide. Only 3.3 kJ/mol less favorable than **n** is the formal base-adduct **m**, while

(50) Additional Mims ENDOR measurements do not support an alternative assignment of these peaks, a ν_+/ν_- doublet from a weakly coupled ^{15}N.

(51) Mims pulsed ENDOR spectra (not shown) further show the presence of both ^{13}C and ^{15}N with coupling(s) on the order of 0.5 MHz or less.

Table 2. Summary of Calculated and Experimentally Obtained Spin Dipolar Couplings for Radical II[a]

nuclei	A_{iso} (cal.)	T_x (cal.)	T_y (cal.)	T_z (cal.)	A_x (exp.)	A_y (exp.)	A_z (exp.)
C1′−^{1}H	+8.3	−0.846	−0.752	1.598	10.0	7.7	7.7
C4′−^{1}H	+8.3	−0.985	−0.619	1.604	10.7	n.d.	13.6
C5′−^{1}H$_\alpha$	−0.3	−0.721	−0.444	1.164		∼0.5	
C5′−^{1}H$_\beta$	−0.3	−0.849	−0.429	1.278			
^{13}C1′	−3.7	−0.313	−0.296	0.609	−5.2	−5.2	−4.3
^{13}C2′	−0.7	−7.539	−5.812	13.350	−7.7	−6.2	n.d.
^{13}C3′	−2.0	−6.497	−4.788	11.286			
^{13}C4′	−4.0	−0.269	−0.197	0.466	−5.2	−5.2	−4.3
^{13}C5′	+4.8	−0.488	−0.293	0.781			
^{15}N1	−3.0	0.335	0.231	−0.566	2.9	2.9	3.4
^{15}NH$_2$	−0.009	0.013	0.006	−0.018		<0.2	
^{15}N3	−0.12	0.067	0.056	−0.122			

[a] All values are in Gauss. The values of A_y (C4′−^{1}H) and A_z (^{13}C2/3′) are not determined by experiment.

the localized radical cations **l** and **m** are 42.5 and 49.8 kJ/mol less stable. None of these four systems fits very well with the experimentally measured spectroscopic data, the smallest deviation being present in radical cation **m**. A survey of g-factor data for systems **a**−**n** (see Table 1) shows that g_{av} values are usually smaller than measured experimentally. Sufficiently high values of g_{av} only result for those systems in which the unpaired spin localizes on highly oxidized carbon centers.

This observation inspired further calculations on the more highly oxidized substrate radicals **o** and **p** that derive from **a** through formal elimination of H_2. The g-factor data for **o** are indeed significantly larger than those of **a**, and show a large hyperfine coupling to H(C1′) and a small coupling to H(C4′). The situation is similar in **p**, but reverses the size of the hfc values for H(C1′) and H(C4′). Rapid exchange between **o** and **p** through hydrogen transfer between the oxygen atoms at C2′ and C3′ may thus generate an average spin distribution at C2′ and C3′, which effectively generates the experimentally observed hfc data. This type of intermediate has been observed in dioldehydratases and recent calculations by Radom et al.[52] indicate that the barrier for interconversion between the localized tautomeric forms drops substantially in the presence of neutral and basic residues and practically vanishes in the presence of anionic residues. Deprotonation of **o/p** may thus generate a delocalized spin system across C2′ and C3′, thereby avoiding the need for any assumptions with respect to the rate of interchange of two tautomeric forms of the substrate radical.

Calculations on the corresponding semidione radical anion were performed in the presence of a water molecule in order to provide a hydrogen bonding environment for the charge-carrying oxygen atoms. The spectroscopic values predicted for radical anion **q** are highly similar to those observed experimentally, giving particularly good agreement with the g-factor anisotropies.

Further agreement between experiment and theory can be derived from analysis of spin dipolar couplings for the most relevant hydrogen atoms. The smaller of the experimentally measured isotropic couplings of 8.5 G shows a notable anisotropy with $A_x = 10.0$ G, and $A_y = A_z = 7.7$ G. Combination of the calculated isotropic coupling for C1′−^{1}H of +8.3 G with the anisotropic spin dipolar couplings calculated for this nucleus (Table 2) yields $A_x = 9.90$ G, and $A_y = 7.45$ and $A_z = 7.55$ G, in practically quantitative agreement with the experiment. Similar isotropic and dipolar couplings have been calculated

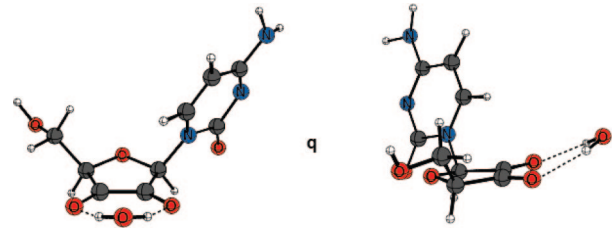

Figure 7. Front and side view of radical an ion **q** (optimized at UB3LYP/TZVP level).

for the hydrogen at C4′ position, also in reasonable agreement with the experiment, but in this case the calculation is ∼3 G too low.

Uniform ^{13}C-substitution in **q** is predicted to lead to small isotropic hyperfine coupling interactions with the carbons in the ribose moiety (C1′: −3.7 G, C2′: −0.7 G, C3′: −2.0 G, C4′: −4.0 G, C5′: +4.8 G), while there are practically no interactions with the carbon atoms in the cytosine base. The ^{14}N nuclei in the base lead to substantial isotropic hfc interactions only from the N1 position (2.16 G), but not from the other two positions (0.08 G from N3 and 0.007 G from NH_2(C4)). Assuming a conversion factor for ^{14}N/^{15}N coupling constants of −1.4028, this equates to an isotropic ^{15}N hfc interaction of −3.04 G at the N1 position. The spin dipolar couplings for carbon and the nitrogen centers in **q** are summarized in Table 2. The two carbon atoms carrying most of the unpaired spin density, C2′ and C3′, have not only small isotropic hyperfine couplings, but show large anisotropies in their couplings. C1′ and C4′, adjacent to C2′ and C3′, as well as C5′ show somewhat larger isotropic couplings and have, in contrast, much smaller anisotropic dipolar couplings.

The most remarkable structural characteristic of radical **q** (Figure 7) is the almost perfectly planar arrangement of the ribose ring carbon atoms with d(C1′−C2′−C3′−C4′) = 0.6°. The oxygen atoms attached to carbon atoms C2′ and C3′ deviate from this plane by no more than 1°. The ribose ring oxygen extends from this plane slightly upward with d(O−C1′−C2′−C3′) = +5.8°.

The electronic structure of **q** is fully compatible with the delocalized Lewis structure shown in Figure 6 with spin density coefficients of 0.21 and 0.18 at the C2′ and C3′ carbon atoms. The remaining part of the unpaired spin density is distributed over the two oxygens attached to the C2′ and C3′ atoms with spin density coefficients of 0.30 and 0.27, respectively.

Testing the Correspondence Between EPR/ENDOR Experiments and the Proposed Structure. ENDOR. A test of structure **q** is provided by comparison of the hyperfine parameters measured by ENDOR spectroscopy and those calculated theoretically. The calculated ^{15}N1 coupling for **q** is very similar to the largest ^{15}N coupling observed experimentally, and the calculated coupling for the ^{15}N3 and $^{15}NH_2$ (largest principal values 0.7 and 0.1 MHz, respectively) could account for the very small couplings observed in Mims ENDOR. The calculation suggests that all five ^{13}C atoms of the ribose should have easily observable couplings, which can be divided into two types. C1′, C4′ and C5′ have similar, largely isotropic dominated couplings of 10−14 MHz. C2′ and C3′ have similar dipolar dominated couplings with T ∼16−19 MHz. A simulation carried out using the calculated tensors is remarkably close to the experimental data, Figure 3 **SM**. With slight adjustments to the values, one tensor of each type may be used to reproduce the spectrum. The adjusted simulation shown in Figure 3 **SM**

(52) Sandala, G. M.; Smith, D. M.; Coote, M. L.; Golding, B. T.; Radom, L. *J. Am. Chem. Soc.* **2006**, *128*, 3433–3444.

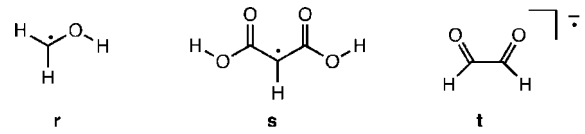

r s t

Figure 8

Table 3. ^{13}C Isotropic and Dipolar[a] Couplings in Methanol Radical (**r**), Malonic Acid Radical (**s**), and Semidione Radical Anion (**t**)

nuclei		a_{iso} [MHz]	T_x [MHz]	T_y [MHz]	T_z [MHz]
r (C1)	calc.[d]	131.7	−74.5	−73.4	+147.6
	calc.[e]	122	−73	−72	+145
	exp.	128[b]			
s (C2)	calc.[d]	64.7	−65.4	−65.0	130.4
	calc.[e]	69	−63	−63	126
	exp.[c]	93	−50	−70	120
t (C1)	calc.[d]	−5.8	−19.3	−15.0	34.31
	calc.[e]	2	−20	−16	36

[a] Dipolar tensor defined as [-T, -T, 2T]. "Perpendicular" components of rhombic tensors averaged. [b] Reference 54. [c] Cole, T.; Heller, C. *J. Chem. Phys.* **1961**, *34*, 1085. [d] Calculated at UB3LYP/IGLOIII//UB3LYP/B3LYP/6−31G(d) level using the energetically most favorable conformer. [e] Calculated at BLYP/TZ2P level with ADF2007.1 (SCM, Theoretical Chemistry, Vrije Universiteit, Amsterdam, The Netherlands).

is a summation of two ^{13}C tensors of (−)[14.5, 14.5, 12] MHz and [−21.5, −17.5, (26)] MHz, with relative intensities chosen to best match the experimental data. The largest principal value of the dipolar tensor is not determined by the experiment, and was chosen to match the calculated value for C3′. All data obtained from the analysis of the ENDOR spectra are summarized in Table 2 together with the calculated data.

The ^{13}C hyperfine tensors thus arrived at are quite different from earlier experimental studies of reference systems such as malonic acid (A = [30, 30, 210] MHz,[53] or CH_2OH radical (a_{iso} ≈ 130 MHz,[54] Figure 8). Our observation is consistent with a recent report of a semidione radical,[55] in which the ^{13}C hyperfine couplings also appeared to be different from those expected for carbon-centered radicals. This led us to test the validity of the computed tensors for malonic acid and CH_2OH radicals, and of the unsubstituted semidione radical by use of the ADF DFT package as well as *Gaussian 03* to calculate the ^{13}C couplings (Figure 8, Table 3). The hyperfine couplings obtained from both packages for the malonic acid and CH_2OH radicals agreed satisfactorily with experiment and with each other, while the ADF value for the semidione radical are quite similar to those calculated for II with *Gaussian 03*.

The calculated and observed hyperfine tensor of the semidione radical **q** can be rationalized by using the theory of Karplus and Frenkel[56] for the interpretation of the isotropic hyperfine interaction of ^{13}C nuclei in π-organic radicals. The theory considers σ-π bond interactions which polarize both the 1s and 2s electrons of the observed carbon atom. These polarization effects are caused not only by the spin density on the "observed" ^{13}C nucleus, but also by neighboring atoms on which unpaired spin density is present, leading to polarization contributions of different signs that partially cancel each other. For a sp^2 hybridized carbon atom that is bonded to three atoms X_i (i = 1, 2, 3), the isotropic ^{13}C hyperfine constant a^C has the form:

$$a^C = \left(S^C + \sum_{i=1}^{3} Q_{CXi}\right)\rho^C + \sum_{i=1}^{3} Q_{XiC}\rho^i \qquad (1)$$

where ρ^C and ρ^i are the π-electron spin densities on the atom C and X_i respectively. The contribution of the 1s electrons is determined by S^C and that of the 2s electrons by the Q_{AB}s, where the index AB denotes the contribution of the polarized bond between the atoms AB due to the spin density on the atom A. Using the above formula with the constants $S^C = -12.7$ G, $Q_{CC'}$ = 14.4 G and $Q_{C'C} = -13.9$ G from Karplus[56] and our calculated spin density distribution on the semidione radical **q** of $\rho^{C2'} = 0.21$, $\rho^{C3'} = 0.18$ and ρ^O at C2′, C3′ = 0.3 and 0.27 respectively, we arrive at $a^{C4'} = Q_{C3'C4'} * \rho^{C3'} \approx -2.5$ and similarly $a^{C1'} = -2.9$ since only one term of eq. 1 is nonzero. These values are very close to the calculated and experimental values reported here. For an estimate of a^C at C2′ and C3′, the coefficients Q_{CO} and Q_{OC} are required which are unknown. However, if all other values are inserted, we arrive at the expression: $a^{C3'} = 0.3 + Q_{C3'O} \cdot 0.18 + Q_{OC3'} \cdot 0.27$. As Q_{CO} and Q_{OC} might have similar values but opposite signs, just as $Q_{C'C}$ and $Q_{CC'}$, here too the contributions likely would cancel, leading to an almost vanishing ^{13}C isotropic hyperfine coupling at O-bonded carbon atoms carrying the spin density. This suggestion is in agreement with our observation and demonstrates the difficulties of predicting ^{13}C hyperfine couplings *a priori*, for a radical whose structure is not known. Finally, it remains difficult to rationalize the predicted positive isotropic hyperfine coupling on C5′. Since C5′ is not part of the π-radical semidione fragment, the positive value of a^C may arise from a more complex polarization mechanism.

EPR. The ^{13}C ENDOR measurements exhibit two different ^{13}C signals, but do not indicate how many ^{13}Cs correspond to each individual signal. Given the narrow and well-defined features for these signals, if one were to arise from two ^{13}C nuclei, their couplings would have to be essentially identical (<1 MHz difference in principle values). Examination of the computation results suggests that C1′,4′, 5′ and C2′, 3′ of the proposed model have sufficiently similar tensors that they might (accidentally) be even more similar in reality, and show unresolved ENDOR signals.

To help count the number of ^{13}Cs that contribute to the ^{13}C ENDOR signals, and thereby test the validity of the proposed model, X-band EPR spectra from the natural-abundance (Figure 2a) and [U−^{13}C/^{15}N] labeled samples (Figure 4 **SM**) were carefully simulated. The experiment was carried out at X band so that broadening of the spectrum due to g dispersion is minimized; by carrying out the experiments at 80 K, interference from the rapidly relaxing Y• is eliminated.

Simulation of the X-band CW spectrum obtained with unlabeled CDP was first carried out to establish an inherent line width. A good fit (not shown) was obtained using the ^{1}H and ^{14}N hyperfine couplings established by ENDOR, plus the small C5′−^{1}H calculated couplings, which had little effect on the simulation. The simulation established a maximum line width of ∼5.0 G. Simulations of the spectrum of [U−^{13}C/^{15}N] CDP (Figure 4 **SM**) were then performed by including the $^{14/15}$N replacement and two or more ^{13}C couplings, as required by ENDOR; simulations were done with up to two of the dipolar type, and up to three of the isotropic type. Simulations with only two ^{13}C were poor, showing more structure to the spectrum than observed and/or insufficient peak to peak width of the spectrum, depending on the choice of intrinsic line width. Adding a second dipolar coupling into the simulation improves the fit substantially. The peak to peak width is a much better

(53) Cole, T.; Heller, C. *J. Chem. Phys.* **1961**, *34*, 1085–1086.
(54) Fischer, H. In *Free Radicals*; Kochi, J. K., Ed.; John Wiley & Sons: 1973; Vol. II, pp 435−491.
(55) Aband, A.; Bandarian, V.; Reed, G. H.; Frey, P. A. *Biochemistry* **2000**, *39*, 6250–6257.
(56) Karplus, M.; Fraenkel, G. K. *J. Chem. Phys.* **1961**, *35*, 1312–1323.

match, as is the line shape, provided that the line width used is near the upper bound suggested by the unlabeled simulations, and noncoaxial tensors are used. Finally, including one or both of the two remaining isotropic couplings arguably improves the fit further, and allows a smaller line width to be used. The EPR simulations thus support the quantum chemical computation in showing that (at least) three ^{13}C nuclei have large couplings, and confirm that there is an accidental equivalence of the ^{13}C that is permitted, but not actually indicated, by the computations.

Discussion

The experiments with E441Q-R1 provided the first mechanistic insight into the intermediates involved in reductive half-reaction of the nucleotide and formation of the disulfide (Scheme 1) in the RNR catalyzed reaction.[13] Our mechanistic model predicted that this mutation would likely slow down the conversion of NDP to **2** as E441 could no longer function as a general base catalyst and would prevent the reduction of **3** to **4**, as the electron transfer from the disulfide radical anion requires concomitant protonation of the 3′-ketone oxygen.[6,14,15] E441Q mutation removes the proton source and hence the disulfide radical anion should and does accumulate. While the spectroscopy is sufficient to firmly establish formation of a disulfide radical anion, the kinetic connection to the normal mechanism of reduction is absent. We hoped that the kinetic relationship between this radical (**I**) and radical **II** would provide further support for the functional role of the disulfide radical anion. The initial studies of Perrson reported that the first radical gave rise to the second radical.[11] Thus determination of the structure of the second radical, established to be nucleotide based by Perrson, was important.[12] Our current studies confirm that the new radical is in fact nucleotide based. The data, however rule out many mechanistically interesting radicals and are most consistent with structure q (Figure 6), an unexpected result. This species is very unlikely to be on the normal catalytic pathway.

While we have not carried out an extensive kinetic analysis of this reaction, it now seems unlikely that there is a direct kinetic connection between the two radicals as originally proposed.[11] The question is then raised as to whether the radicals occur within the same or in parallel pathways. If the radicals occur within the same pathway, the disulfide radical anion, in equilibrium with the thiyl radical/thiolate, has limited reactivity options. With the E441Q mutant, electron transfer cannot occur to ketone **3** (Scheme 1), as this step requires concomitant protonation to make the reaction thermodynamically feasible.[14,15] Thiyl radicals can add to carbonyls and can also mediate hydrogen atom abstraction such as the C4′-radical formation (**5**, Scheme 2) we originally proposed. Neither of these options, however, gives rise to a nucleotide radical structure consistent with our EPR and ENDOR spectroscopy. In a preliminary kinetic experiment, there appears to be no lag phase in the production of radical II. A lag phase would be expected if radical II is on the same pathway as I, given the complex chemistry required to generate **q** (Figure 6) from **1** (Scheme 1). Instead radical II is present in the earliest time points (200 ms), suggesting that it is most likely generated in a parallel reaction sequence and is off pathway from the normal reaction.

The difficulties in identifying radicals generated on the second time scale in RNR has previously been observed with the nitrogen centered radical formed on inactivation of *E. coli* RNR with 2′-azido-2′-deoxynucleotide.[57] The chemistry occurs within a closed active site cavity and is unlikely to be recapitulated in homogeneous solution. In the case of the nitrogen centered radical, this species is at least three steps from the initial 3′ hydrogen atom abstraction and the observed radical is very stable. In the case of radical II, one possibility is that the observed nucleotide radical is also many steps removed from the initial 3′ radical (**1**, Scheme 1), with the resulting radical also being very stable.

Several experiments, in addition to our spectroscopic analysis, support the assignment of structure **q** (Figure 6) to the radical II. The first is the recent report from the Frey and Reed laboratories that hydroxyacetaldehyde inactivates the adenosylcobalamin requiring dioldehydratase, giving rise to a stable radical whose structure is proposed to be analogous to II.[55] Unfortunately this radical interacts with cob(II)alamin and thus the detailed hyperfine interactions have not been reported. Second, 2′,2″ difluoro-2′-deoxycytidine 5′-triphosphate is a potent mechanism based inhibitor of all ribonucleotide reductases we have examined.[23] Inactivation of the *Lactobacillus leichmannii* ribonucleoside triphosphate reductase with this analog resulted in trapping with NaB^2H_4 of a 2′, 3′ diketone nucleotide.[23] During the course of the enzymatic inactivation, two fluorines were lost, an "oxygen was added" and an oxidation of the nucleotide occurred! Thus, as noted above, the chemistry in the active site cavity is very complex. One possible mechanism is that oxygen addition must also be occurring to a cytidine intermediate with the E441Q mutant to generate radical II. Initially we thought that a radical such as **2** (Scheme 1) or **5** (Scheme 2) might be trapped by O_2, however, Persson in their original paper reported that both radicals I and II were produced under anaerobic conditions.[12] Thus the mechanism by which an additional oxygen, presumably derived from water, is incorporated into the nucleotide is not understood and is likely many steps removed from the initially generated radicals.

Another possibility is that RNR is partially oxidized. This state along with altered general base/acid chemistry associated with the E441Q substitution, might allow **1** (Scheme 1) to be oxidized directly by the active site disulfide. Our previous studies with a mechanism based inhibitor, 2′-chloro-2′-deoxynucleotide showed that 3′ hydrogen atom abstraction could occur with oxidized RNR.[45] However, the mechanism by which hydrogen atom abstraction by the putative thiyl radical (C225) on the α face of the ribose to give **q**, remains a challenge due to stereochemistry. This proposed pathway requires that a substantial amount of RNR is in the oxidized state, despite the fact that enzyme is prereduced directly before each experiment and that 10 mM DTT is present during the inactivation.

In conclusion, the present paper describes another example[57] of the difficulty in assigning a structure to a radical detected in an enzymatic reaction that occurs within an enzyme active site, when rerouted from normal catalytic pathway either by a mutation of the protein (E to Q) or the substrate. It also demonstrates the power of combining high field spectroscopic EPR and ENDOR spectroscopic methods in conjunction with computational methods, to elucidate such a structure.

(57) Fritscher, J.; Artin, E.; Wnuk, S.; Bar, G.; Robblee, J. H.; Kacprzak, S.; Kaupp, M.; Griffin, R. G.; Bennati, M.; Stubbe, J. *J. Am. Chem. Soc.* **2005**, *127*, 7729–7738.

Acknowledgment. We thank H. Schwalbe and D. Blechschmidt for ^{15}N and ^{13}C CDP; T. Argirevic and M. Seyedsaymdost for development of the expression system for E441Q-α; and B. Giese for his suggestions of possible structures of radical II. Funding support for H.Z. SPP 1071, M.B., DFG IRTG1422; J.S., NIH GM29595; B.M.H., H13531; and R.G.G., EB002804 and EB002026 is acknowledged. We also thank the reviewers for their thoughtful comments.

Supporting Information Available: Synthesis of [4′-^{2}H] CDP; Synthesis of [5′, 5′′-^{2}H] CDP; Simulation of the ^{15}N and ^{13}C ENDOR spectra; 9 GHz pulsed EPR spectrum and simulation; 35 GHz Mims pulsed ENDOR spectra of ^{13}C /^{15}N CDP. This material is available free of charge via the Internet at http://pubs.acs.org.

JA806693S